강재 골조의 비선형 지진해석을 위한 합성 보 요소

Composite Beam Element for Nonlinear Seismic Analysis of Steel Frames

김 기 동[1] · 고 만 기[1] · 이 규 세[2] · 황 병 국[3]
Kim, Kee Dong *Ko, Man Gi* *Yi, Gyu Sei* *Hwang, Byoung Kuk*

요 약 : 지진 하중에 대한 강재 모멘트 골조의 합성 슬래브를 포함한 강재 보의 비탄성 거동을 모델하기위한 합성 보 요소가 제안되고 강재 모멘트 골조의 지진 거동에 대한 합성 슬래브의 효과가 조사된다. 합성 보 요소는 단일 직렬 힌지 모델로 간주 될 수 있고, 그 해석 결과는 실험결과와 매우 합리적인 상관 관계를 보였다. 합성 보 요소는 기존의 강재 보 요소보다 상당히 좋은 거동을 보이고, 합성모델은 지진 하중 하에서의 구조물의 국부변형과 전체 응답을 기존의 강재 모델보다 정밀하게 예측할 수 있다. 합성 슬래브는 강재 모멘트 골조의 국부 및 전체 해석 응답에 상당히 큰 효과를 나타낸다.

ABSTRACT : This study presented a composite beam element for modeling the inelastic behavior of the steel beam, which has composite slabs in steel moment frames that are subjected to earthquake ground motions. The effects of composite slabs on the seismic behavior of steel moment frames were investigated. The element can be considered as a single-component series hinge type model whose predicted analytical results were consistent with the experimental results. Likewise, the element showed a significantly better performance than the bare steel beam elements. The composite model can also predict more accurately the local deformation demands and overall response of structural systems under earthquake loading compared with the bare steel models. Therefore, composite slabs can significantly affect locally and globally predicted responses of steel moment frames.

핵 심 용 어 : 합성 보 요소, 합성 슬래브, 지진 운동, 강재모멘트 골조
KEYWORDS : composite beam element, composite slab, earthquake ground motion, steel moment frame

1. GENERAL

Moment resisting frames (MRFs) designed according to current building codes (International 1997: Structural 1996) are expected to deform well into the inelastic range during severe earthquake ground motions. The design philosophy for seismic resistant steel MRFs adopted by building codes discourages the formation of plastic hinges in the clear span portion of columns, while encouraging the formation of hinges in beams or in beam-column joints. Thus, accurate modeling of random cyclic inelastic response of members subject to bending, but without significant axial force (i.e., beams), is essential for accurate modeling of MRF response. The accurate modeling of inelastic response of beams during earthquake excitations depends on the development of reliable analytical elements which describe the hysteretic behavior of the critical regions at the ends of beams. The development of such an analytical model for composite beams and its application are the subject of this study.

While beams in moment frames are usually designed as bare steel member action under lateral

1) 정회원, 공주대학교 토목환경공학과 교수, 공학박사
2) 정회원, 선문대학교 토목환경공학과 교수, 공학박사
3) 정회원, 공주대학교 토목환경공학과 박사과정, 구조기술사

본 논문에 대한 토의를 2003년 4월 30일까지 학회로 보내주시면 토의 회답을 게재하겠습니다.

loads, significant composite action can exist due to shear studs that are provided to transfer diaphragm forces and/or welds that attach the metal deck to the beams. Additionally, at the beam-column connection the slab can have a significant impact on the local force transfer and the behavior of the connection and panel zone. Composite beam action is one of several effects that increase the stiffness of the structure and contribute to more accurate calculation of the characteristic vibration frequencies. In Fig. 6, the overall response predicted by an analysis modeling the composite beams using the multi-linear hinge element for bare steel beams (Kim 2000) is compared with the experimental data (Wenk 1977). From this figure, it can be seen that by ignoring the effect of the concrete slab, the overall stiffness and strength of the test frame are significantly underestimated. If the composite beam action is likely to exist whether or not the frame is designed compositely, composite action should be considered to more accurately predict the overall and local behavior of MRFs under earthquake motions.

A composite beam shows complex behavior due to slip between the concrete slab and the steel beam, and the variation of longitudinal stress across the width of the slab, which is dependent on the joint details and the loading pattern. To ideally model the behavior of composite beams during earthquake loading, these factors should be considered. A three-dimensional finite element analysis can most accurately model the behavior of composite beams, but it is computationally inefficient for inelastic earthquake analysis of multistory MRFs. Also, the behavior of shear connectors is not fully understood, especially under arbitrary cyclic loading, even though many researchers (Slutter et al. 1965; Ollgaard et al. 1971; Grant et al. 1977) have studied the behavior of shear studs under monotonic loading. And it is also very difficult to define the crushing effect of concrete at a joint on the stiffness and strength of beams, and the bonding behavior between reinforcing bars and concrete under arbitrary cyclic loading.

Modeling of the seismic response of composite beams by a two-dimensional structural element is a difficult task. The longitudinal membrane stress is not uniform across the width of the concrete slab. The effective width, which accounts for the non-uniform longitudinal stress pattern, varies along the beam, and changes as the moments in the beam change during loading history. Since the non-uniform effective width along the length of the beam changes during the loading history, a two-dimensional model that employs the stress-strain or moment-curvature relation does not warrant the exact prediction of the response of composite beams. Moreover, a measure of inelastic behavior in terms of strains and curvatures can be problematic because they are not directly converted into equivalent plastic rotations that are a more common measure of ductility demands in frames.

Some researchers (Ricles 1987; Lee 1987) have developed two-dimensional discrete member elements as a compromise between simplicity and accuracy, which employ a hysteretic model describing the moment-rotation relationships of composite beams. In these models, it is assumed that the influence of slip and the variation of longitudinal membrane stress on the behavior of composite beams can be implicitly included in the moment-rotation relationships of composite beams. In this study, based on observations from the experimental behavior of composite beams and existing composite beam models, a composite beam element is developed. The element can be considered as an one-component series hinge type model. It employs nonlinear force-deformation relationships and accounts for the influence of a moving inflection point on the beam element stiffness. This element is intended to represent the clear span portion of beams in steel moment frames, and does not consider the geometric nonlinearity effects.

2. GENERAL DESCRIPTION

The two dimensional composite beam element consists of a linear elastic composite beam element with a nonlinear hinge at each end. To facilitate the discussion, this element will be referred to as the

"complete element," consisting of both hinges and the elastic composite beam element. The hinges are considered to have zero length. Inelastic behavior due to yielding under moment is concentrated in the hinges. Both hinges are assumed to be initially rigid. Therefore the initial stiffness of the complete element is that of the elastic composite beam element. As the forces at the element ends increase, the hinges can yield, resulting in a reduced stiffness of the complete element. Under increasing deformation, the hinge strains harden, following the nonlinear force-deformation relationships.

Each hinge possesses nonlinear rigid-plastic moment-rotation relationships in an attempt to more closely mimic experimentally observed behavior. To produce a reduced stiffness for the complete element at any load step after yielding, the instantaneous tangent flexibility of the nonlinear rigid-plastic force-deformation relationships for a hinge are combined with the flexibility for the elastic composite beam element.

Since the behavior of composite beam varies according to the direction of moment due to non-symmetric section, a hinge should discern the load paths to model the hysteresis behavior of composite beam for arbitrary cyclic loading. Hysteretic rules employed for this composite beam element, which take into account the influence of non-symmetric section, strength deterioration, stiffness degradation, and so forth, guide a hinge to discern the load paths and to follow the specified nonlinear moment-rotation relationships.

3. DEGREES OF FREEDOM

The complete element has two external nodes and two internal nodes. The internal nodes exist at the end of the elastic element. The hinges connect the internal nodes with the external nodes. The external nodes connect to the global structure and each have three degrees of freedom, namely translations and rotation in the local coordinate system, as shown in Fig. 1. In the local coordinate system, if the rigid body motions are removed, the element can be considered as a simply supported beam. On the basis of equilibrium, all the components of local nodal forces $\mathbf{R}$ (R_1 to R_6) can be computed from the values of relative forces $\mathbf{s}$ (s_1, s_2, and s_3). The transformation from the relative forces $\mathbf{s}$ to the nodal forces $\mathbf{R}$ is defined as

$$\mathbf{R} = \mathbf{A} \cdot \mathbf{s} \tag{1}$$

where $\mathbf{A}$ is the force transformation matrix, which is well known and can be found in the literature (Przemieniecki 1968). From geometry, the transformation from the local displacements $\mathbf{r}$ to the relative deformations $\mathbf{v}$ (v_1, v_2, and v_3) is accomplished by

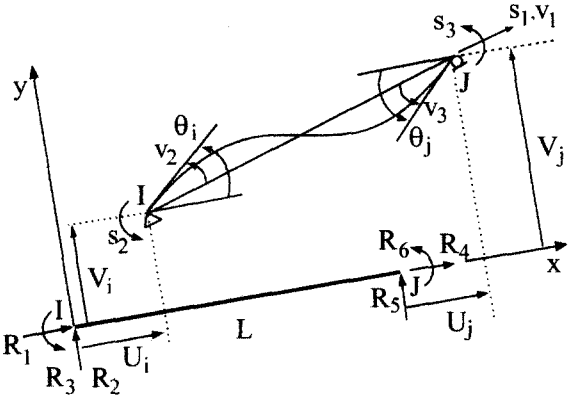

Fig. 1 Element Relative Forces and Deformations in Local Coordinate System

$$\mathbf{v} = \mathbf{A}^{T} \cdot \mathbf{r} \tag{2a}$$

where $\mathbf{r}^{T} = \{U_i, V_i, \theta_i, U_j, V_j, \theta_j\}$ (2b)

4. COMPLETE ELEMENT STIFFNESS

A flexibility matrix $\mathbf{f}$ is first formed for the elastic element which includes the effects of shear, as follows:

$$\mathbf{dq} = \mathbf{f} \cdot \mathbf{ds} \tag{3a}$$

where $\mathbf{dq}$ (dq_1, dq_2, and dq_3) is the elastic deformation increment at the internal nodes and $\mathbf{ds}$ is the action

increment, in which

$$\mathbf{ds}^{T} = \{dF, dM^{I}, dM^{J}\} = \{ds_1, ds_2, ds_3\} \qquad (3b)$$

For the hinges at nodes I and J, the incremental action-deformation relationship can be expressed as

$$\mathbf{dw}_p = \begin{Bmatrix} 0 \\ d\theta_p^I \\ d\theta_p^J \end{Bmatrix} = \begin{Bmatrix} dv_1 - dq_1 \\ dv_2 - dq_2 \\ dv_3 - dq_3 \end{Bmatrix} = \mathbf{f}_p \cdot \mathbf{ds} \qquad (4)$$

where $\mathbf{dw}_p$ is the vector of plastic hinge deformations at nodes I and J, $d\theta_p^I$ and $d\theta_p^J$ are the incremental plastic rotation at nodes I and J, and $\mathbf{f}_p$ is the hinge or plastic flexibility matrix in which nonzero terms are the second and third elements in diagonal. Using Eqs. 3a and 4, the action-deformation relationship is obtained for the complete element expressed in terms of the degrees of freedom $\mathbf{v}$.

$$\mathbf{dv} = \mathbf{dq} + \mathbf{dw}_p = \mathbf{F}_t \cdot \mathbf{ds} \qquad (5)$$

The hinge flexibility coefficients of $\mathbf{f}_p$ can be simply added to the appropriate coefficients of the elastic element flexibility matrix $\mathbf{f}$ in order to obtain the tangent flexibility matrix $\mathbf{F}_t$ for the complete element. Having determined the 3x3 tangent flexibility matrix $\mathbf{F}_t$, this matrix is inverted to obtain a 3x3 tangent stiffness matrix $\mathbf{K}_t$.

5. HYSTERETIC RULES

Hysteretic rules are basically intended to take into account the effect of concrete slab on the hysteresis behavior of steel beam, and are determined from the observation of available experimental data and the modification of the existing models (Ricles 1987; Lee 1987). For monotonic loading, two bilinear moment-rotation relationships as shown in Fig. 2a are employed to consider non-symmetric section and the early crack of concrete slab under the negative moment. For cyclic loading, the basic cyclic moment-rotation relationships of steel beam are modified to consider the effect of concrete slab according to crack closing and opening as shown in Fig. 2b.

The basic parameters to describe the monotonic moment-rotation relations are elastic stiffness, inelastic stiffness, and yield moment for positive and negative moments, respectively. These parameters are determined through calibration to available experimental data (Uang 1985; Lee 1987; Tagawa 1986, 1989).

The elastic stiffness of an equivalent cantilever composite beam representing the length from the one end of beam to the inflection point under a linear moment distribution is $K_e^+ = 3EI^+/L^+$ and

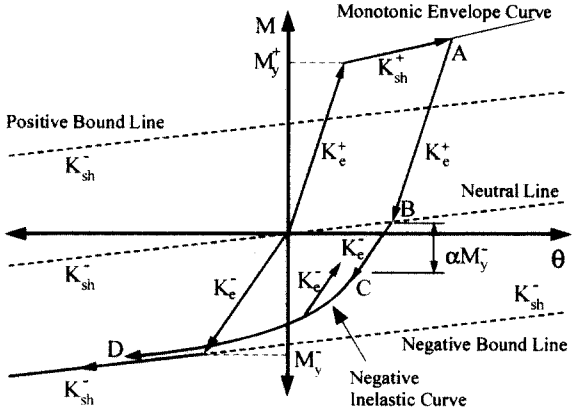

a) Monotonic model and Stiffness Degradation for Negative Moment

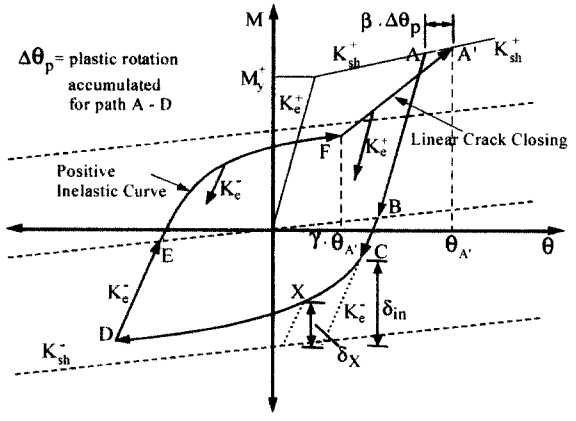

b) Stiffness Degradation and Pinching for Positive Moment

Fig. 2 Proposed Hysteretic Moment-Rotation Model of Composite Beam

$K_e^- = 3EI^-/L^-$ for each of positive and negative moments in which L^+ and L^- are the length of equivalent cantilever beam under positive and negative moments, respectively. It should be noted that the term elastic of the negative elastic stiffness is used to represent the elastic behavior of steel beam after the early crack of concrete slab under the negative moment. The strain-hardening stiffnesses for positive and negative bending moments are expressed as fractions of the respective elastic stiffnesses as follows: $K_{sh}^+ = 0.025 \cdot K_e^+$ and $K_{sh}^- = 0.05 \cdot K_e^-$.

The effective width of the concrete slab b_{eff} on each side of the beam center-line for computing positive elastic stiffness is determined by the minimum of $L/8$, $b_o/8$, and b_{es} (LRFD Specification 1994) in which L is the beam span, center to center of supports, b_o is the distance from the beam center-line to the center-line of the adjacent beam, and b_{es} is the distance from the beam center-line to the edge of the slab. Using the effective concrete slab width, the moment of inertia of a composite section I_{tr} is calculated. To account for the influence of slip between the concrete slab and the steel beam on the positive elastic stiffness, the moment of inertia I^+ applied to the positive elastic stiffness is assumed to be a fraction of I_{tr}. From the available experimental results, it has been found that I^+ equal to $0.85 \cdot I_{tr}$ is reasonable. To obtain the moment of inertia I^- used for the negative elastic stiffness, the steel beam section and reinforcing steel bars within the effective slab width are considered.

The negative yield moment M_y^- of the monotonic model shown in Fig. 2a is the plastic moment of both the steel beam section and reinforcing steel bars within the effective width. The positive yield moment M_y^+ is assumed to be a fraction of the ultimate moment at the connection, which can be estimated based on the plastic stress distribution. The contribution of the concrete slab to the ultimate moment M_{max}^+ at the connection is determined by using the column width b_{cf} and the concrete compressive bearing stress of $1.3f_c'$ due to the confinement of concrete near the column (duPlessis et al. 1973). For the exterior joints, the plastic neutral axis is determined by solving the following equation for compressive steel area, A_{sc} :

$$2A_{sc}F_y = A_sF_y - 1.3f_c'b_{cf}t_c - A_rF_{yr} \tag{6a}$$

From Eq. 6a, the ultimate moment at the connection is written as

$$M_{max}^+ = 1.3f_c'b_{cf}t_cy_n\left(1-\frac{t_c}{2y_n}\right) + A_{sc}F_yy_{sc} + (A_s-A_{sc})F_yy_s + A_rF_{yr}y_r \tag{6b}$$

where y_n = distance from the plastic neutral axis to the top surface of the slab; y_{sc} = distance from the plastic neutral axis to the compression resultant of steel; y_s = distance from the plastic neutral axis to the tension resultant of steel; y_r = distance from the plastic neutral axis to the compression resultant of reinforcing bars; b_{cf} = column flange width; t_c = concrete slab thickness from the top surface to the top of metal deck; A_s = total steel area; A_r = area of reinforcing bars within the effective slab width; F_{yr} = yield stress of reinforcing bars.

To determine the ultimate moment M_{max}^+ at the interior joints, a method based on tension yield of reinforcing bars unlike the exterior joints is employed (Wenk 1977). In this method it is assumed that under lateral loads the reinforcing steels in the positive moment region of an interior joint are governed by the tension yield of reinforcing steels in the negative moment region of the other side. The stress distribution of the composite section in the positive moment region of the interior joint is the same as that of the exterior joint with the exception that the compression force of reinforcing bars is changed into the tension force. The resultant maximum slab force is equal to $1.3f_c'b_{cf}t_c - A_rF_{yr}$. The plastic neutral axis is determined by solving the following equation for compressive steel area, A_{sc}:

$$2A_{sc}F_y = A_sF_y - 1.3f'_cb_{cf}t_c + A_rF_{yr} \quad (7a)$$

From the modified stress distribution and Eq. 7a, the ultimate moment at the interior joint is written as

$$M^+_{max} = 1.3f'_cb_{cf}t_cy_n\left(1-\frac{t_c}{2y_n}\right) + A_{sc}F_yy_{sc} + (A_s-A_{sc})F_yy_s - A_rF_{yr}y_r \quad (7b)$$

From the available experimental data, it has been found that the positive yield moment M^+_y of $0.95M^+_{max}$ is reasonable.

In the hysteretic moment-rotation model of a composite beam shown in Fig. 2, the hysteresis behavior of steel beam is bounded by the positive and negative bound lines, and after crack closing the behavior of composite section is bounded by the positive moment envelope curve. An inclined neutral line, which has the slope K^-_{sh} and passes through the origin of the coordinate system, represents the location of crack opening on the unloading path from the behavior of composite section.

The stiffness degradation in the negative moment region is illustrated in Fig. 2a. The factor α defines the ratio of the negative linear elastic range to the negative yield moment. The factor α is determined empirically by examining the available experimental results and is chosen to be $\alpha=0.5$. Figure 2b shows the stiffness degradation, pinching, and strength deterioration for the positive moment region. The stiffness degradation begins at the inclined neutral line. The effect of pinching and strength deterioration are represented, respectively, by the γ and β factors, which are determined empirically to be $\gamma=0.2$ and $\beta=0.05$. It is noted that whenever the crack starts to close (point F) after the crack opens, the reloading path will follow the linear crack closing line F-A'.

The negative and positive inelastic curves (lines C-D and E-F) are described by the plastic stiffness obtained by using the normalized shape factor $\hat{h}$ (Dafalias 1975). The plastic stiffness K^x_p at an arbitrary point X on the inelastic curve shown in Fig. 2b is a function of the normalized shape factor $\hat{h}$. The plastic stiffness K^x_p is determined from the following equation:

$$K^x_p = K^-_{sh}\left[1+\hat{h}\frac{\delta_x}{\delta_{in}-\delta_x}\right] \quad (8)$$

where δ_{in} is the initial distance between the starting point of the inelastic curve and the corresponding point on the bound line, δ_x is the distance between an arbitrary point X on the inelastic curve and the corresponding point on the bound line, and K^-_{sh} is the plastic stiffness of the bound line. The procedure to determine the normalized shape factor $\hat{h}$ is as follows: i) choose an arbitrary point X such that $1/10 \le \delta_x/\delta_{in} \le 1/2$, ii) calculate the shape factor from $h=\delta_x/\theta^x_p+(\delta_{in}/\theta^x_p)\cdot[\ln(\delta_{in}/\delta_x)-1]$ in which θ^x_p is the plastic rotation at an arbitrary point X, and iii) normalize the shape factor by the plastic stiffness of the bound line $\hat{h}=h/K^-_{sh}$.

By applying the above procedure to the available experimental data, it has been determined that the normalized shape factors, $\hat{h}_p$ and $\hat{h}_n$ were chosen as 10 and 6, respectively, for the positive and negative inelastic curves as shown in Figs. 2a and 2b.

The composite beam element is a one-component series hinge model and has the capability to account for the influence of a moving inflection point on the element stiffness. It is assumed that the inflection point does not change during a small load or time step and the inflection point obtained at the end of the previous load step can be applied to the next load step. At the end of a load step, the inflection point is determined from the linear moment distribution induced by earthquake motions alone, under the assumption that the moment distribution due to the gravity load is not significant when compared with that due to earthquake excitations.

According to the inflection point obtained at the end of the previous load step, the lengths L^I and L^J are determined, where L^I is the length of equivalent

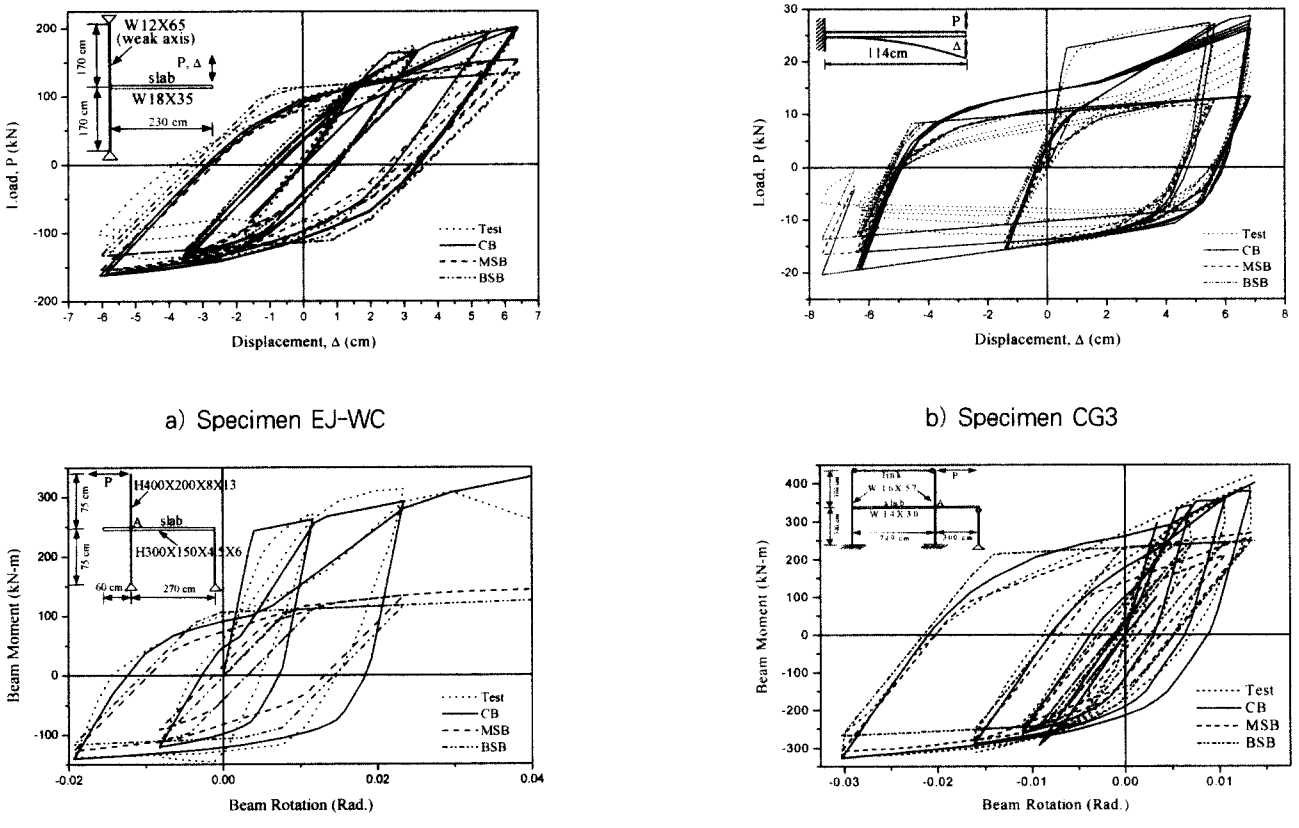

Fig. 3 Comparison of Experimental and Analytical Results

cantilever beam from the beam end I to the inflection point and L^J is the length from the inflection point to the beam end J. It is then assumed to determine the stiffness of the complete element at the current load step that the flexural rigidity of the elastic beam element is the elastic flexural rigidity of the composite beam EI^+, and the two plastic hinges at the member ends I and J represent inelastic flexural deformation within the lengths of equivalent cantilever beam L^I and L^J. Thus, the flexibility of each of the two plastic hinges at the current load step is defined as:

$$f_p^I = \frac{1}{K_p^I} = \frac{1}{K_t^I} - \frac{L^I}{3EI^+} \quad \text{for plastic hinge of end I} \tag{9a}$$

$$f_p^J = \frac{1}{K_p^J} = \frac{1}{K_t^J} - \frac{L^J}{3EI^+} \quad \text{for plastic hinge of end J} \tag{9b}$$

where K_t^I is the tangent stiffness of the hysteresis moment-rotation model based on the equivalent cantilever length L^I, and K_t^J is the tangent stiffness based on the length L^J. It is noted that for the first load step for which the moment distribution is not known, an iteration procedure with the initial guess for the equivalent cantilever lengths is used to obtain proper equivalent cantilever lengths for the following load steps.

6. COMPARISON TO TEST DATA FOR BEAM MEMBERS

To investigate the performance of the composite beam element, analytical results are compared with test results for a small-scale specimen CG3 (Uang 1985), full-scale specimens EJ-WC (Lee 1987), and Tagawa 86 and 89 (Tagawa 1986; 1989). The beam

section properties of the specimens are listed in Table 1 and the other details can be found in the above literatures. In Table 1, I_{steel} and M_p are the moment of inertia and the plastic moment of steel beam, respectively. From this table, it can be noted that relatively shallow beams are used for test specimens and concrete slabs significantly increase the stiffness and strength of beams in the positive moment region.

Figure 3 shows comparisons between composite beam predictions (CB) and test results for the above specimens. Results are also compared with the bare steel elements: the multi-linear beam-column element (MSB) and the bilinear beam-column element (BSB), which is most widely used for inelastic dynamic analysis (Kanaan and Powell 1973) and of which the strain hardening stiffness is taken as 3% of the elastic stiffness.

Figure 3a shows the comparison of experimental and analytical results of Lee's specimen EJ-WC. The specimen was an exterior joint assemblage, and its beam was connected to the column web by connecting plates. The comparison of experimental and analytical results of Uang's specimen CG3 is presented in Fig. 3b. The comparisons of composite beam predictions and experimental results show good agreement until the bottom flange of steel beam develops severe local buckling. The bare steel beam elements provide much lesser strength and stiffness than the experimental results as expected from Table 1. The multi-linear steel beam element shows smoother transition from elastic to inelastic region and little more strength than the bilinear steel beam element.

Table 1. Section Properties of Test Specimens

Specimen	Beam Section	Slab Thickness(cm)	I^+	M_y^+
EJ-WC	W18X35	8.89	$2.5I_{steel}$	$1.9M_p$
CG3	M6X4.4	2.54	$3.0I_{steel}$	$2.1M_p$
Tagawa 86	H300X150 X4.5X6	10	$4.6I_{steel}$	$2.2M_p$
Tagawa 89	W14X30	9	$2.9I_{steel}$	$1.5M_p$

The correlations of the experimental and analytical results for specimens Tagawa 86 and 89 are shown in Figs. 3c and 3d. The analytical and experimental results are the beam moment-rotation relations at point A of the subassemblages shown in Figs. 3c and 3d. In the analysis of specimen Tagawa 86, the yield stress of reinforcing bars was assumed to be that of the steel beam because the yield stress of reinforcing bars was not available. In specimen Tagawa 89 the response of a beam framing into an interior joint was investigated. The agreement between the experimental data and composite beam predictions is reasonable except that for specimen Tagawa 89 the composite beam element overestimates the strength for small amplitudes of rotation even though the ultimate moment based on tension yield of reinforcing bars was applied. The bare steel beam elements significantly underestimate the strength and stiffness of the beams.

From the comparisons, it has been shown that the hysteretic rules of the composite beam element can reasonably model the strength, stiffness, pinching, and stiffness degradation of a composite beam until local buckling of the beam bottom flange occurs. The composite beam element clearly provides significantly better correlation with the test data as compared with the bare steel beam elements. The bare steel beam elements cannot properly provide the increase of strength and stiffness due to concrete slab for shallow beams.

7. COMPOSITE PANEL ZONE ELEMENT

In many practical cases, the panel zone can dominate the inelastic response of a moment frame. It was reported (Lee 1987; Kim 2002) that the presence of a composite concrete floor slab could significantly affect panel zone behavior, particularly for relatively shallow beams. Therefore, accurate panel zone models that can account for the effect of composite slabs on the behavior of panel zones are needed to realistically predict overall frame performance. To take into account the effect of composite slabs on the behavior

of panel zones, a composite panel zone model (Kim 2002) was developed for the monotonic and cyclic behavior of beam-to-column joints in steel moment frames with composite floor slabs. This model is based on the concept of representing the panel zone as a nonlinear rotational spring and can consider the increase in the effective depth of the panel zone due to the presence of the concrete slab. This composite panel zone element combined with the developed composite beam element will be applied to investigate the effects of composite slabs on the behavior of steel subassemblages and frames with concrete slabs.

To investigate the performance of the composite panel zone element (CPZ), analytical results are compared with test results for Lee's specimen EJ-FC (Lee 1987) in Fig. 4. Also shown in this figure are the analytical predictions using the bare steel panel zone elements: the nonlinear steel panel zone element (NPZ) (Kim 2002) and the bilinear steel panel zone element (BPZ), which is most widely used for inelastic dynamic analysis and of which the strain hardening stiffness is taken as 3% of the elastic stiffness. It is clear from Fig. 4 that the composite panel zone element shows much better correlation with the test data than the bare steel panel zone elements for both small and large amplitudes of deformations. The bilinear steel panel zone element substantially underestimates panel zone strength more than the nonlinear steel panel zone element. More extensive comparisons can be found in Kim and Engelhardt (2002).

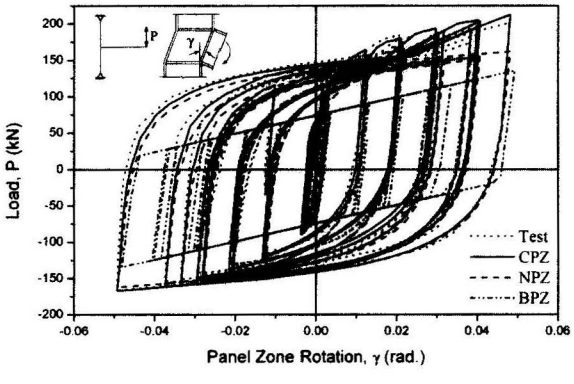

Fig. 4 Comparison of Model Predictions and Test Results for Local Panel Zone Response of Specimen EJ-FC

8. COMPARISON TO TEST DATA FOR ASSEMBLAGES

To investigate the interaction of the composite beam and composite panel zone elements described above, the elements are combined into steel subassemblages and frame with concrete slab, such as Lee's specimens EJ-FC and IJ-FC, Engelhardt's specimens DBWP-C (Engelhardt 2000a) and UTA-FF (Engelhardt 2000b), and a one-story and two-bay frame specimen CA-1 (Wenk et al. 1977). The beam section properties of the specimens are listed in Table 2. From this table, it can be seen that the increase of the stiffness and strength of beams in the positive moment region due to concrete slab is much lesser for specimens DBWP-C and UTA-FF because of the rather deep W36x150 beams used for these specimens than for the other specimens.

Figure 5 shows comparisons between composite model predictions and test results for the overall load displacement response for the above specimens. The composite model (CM) consists of the composite beam and composite panel zone elements, and the multi-linear steel beam-column element. Results are also compared with the bare steel models. In refined bare steel model (RSM), both beams and columns are modeled using the multi-linear steel beam-column element, and panel zones are modeled using the nonlinear steel panel zone element. In basic bare steel model(BSM), both beams and columns are modeled using the bilinear steel beam-column element, and panel zones are modeled using the bilinear steel panel zone element.

Table 2. Beam Section Properties of Test Specimens

Specimen	Beam Section	Slab Thickness(cm)	I^+	M_y^+
EJ-WC	W18X35	8.89	$2.5I_{steel}$	$1.77M_p$
IJ-FC	W18X35	8.89	$2.5I_{steel}$	$1.80M_p$
DBWP-C	W36X150	8.89	$1.2I_{steel}$	$1.08M_p$
UTA-FF	W36X150	8.89	$1.2I_{steel}$	$1.13M_p$
CA-1	W10X19	8.89	$2.8I_{steel}$	$1.60M_p$

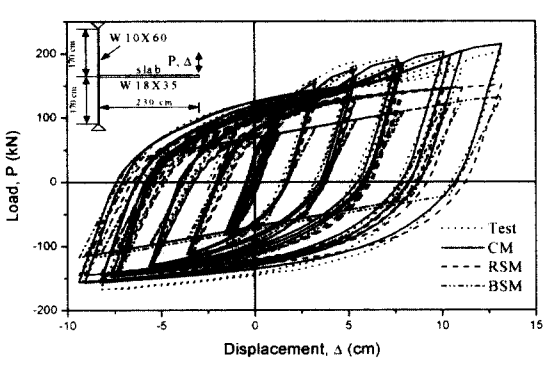

a) Specimen EJ-FC

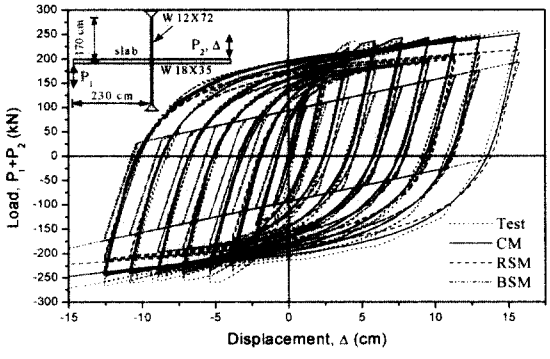

b) Specimen IJ-FC

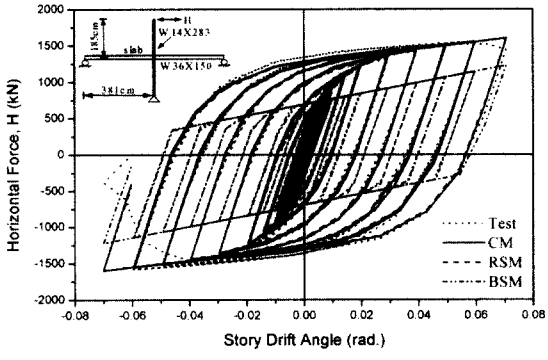

c) Specimen DBWP-C

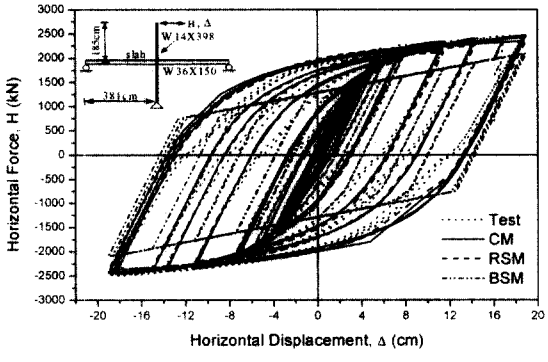

d) Specimen UTA-FF

Fig. 5 Comparison of Model Predictions and Test Results for Overall Response

Figures 5a and 5b show comparisons for specimens EJ-FC and IJ-FC. From these figures, it has been shown that the composite model clearly provides significantly better correlation with the test data as compared with the bare steel models. The bare steel models cannot properly model the experimentally observed behavior due to the effect of composite slab after crack closure. The refined steel model underestimates the overall strength by about 26 % for specimen EJ-FC and by about 15 % for specimen IJ-FC. The bilinear steel model provides much lesser strength than the refined steel model.

In Figs. 5c and 5d, the model predictions are compared with test results for specimen DBWP-C and UTA-FF. The performance of the composite and refined steel models provide reasonable correlation with experimental data. From Table 2 and the fact that the refined steel model prediction matches well with experimental data, it can be deduced that there is little effect of the composite slab on the response of beams due to the rather deep W36x150 beams used for these specimens. Even if the effect of concrete slab is negligible for specimens DBWP-C and UTA-FF, the bilinear steel model substantially underestimates overall strength in the latter cycles of loading.

Figure 6 compares the overall response predicted by the test and the analysis for Wenks specimen CA-1. Since specimen CA-1 was designed for the

Table 3. Plastic Rotations for Specimen UTA-FF

Model	Total Plastic Rotation (rad.)	Panel Zone Plastic Rotation (rad.)	Beam Plastic Rotation (rad.)	Column Plastic Rotation (rad.)
Test	0.033	0.017	0.011	0.005
CM	0.037	0.022	0.015	0.0
RSM	0.037	0.033	0.003	0.0
BSM	0.039	0.038	0.001	0.0

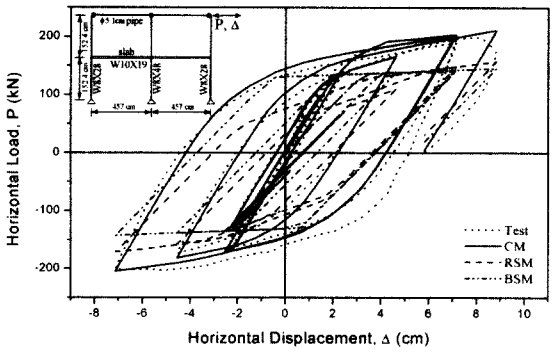

Fig. 6 Comparison of Experimental and Analytical Results of Specimen CA-1.

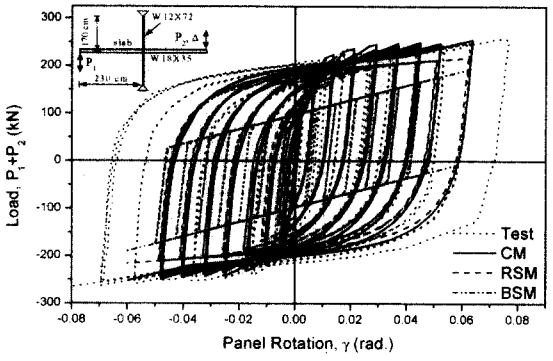

Fig. 7 Comparison of Model Predictions and Test Data for Local Panel Zone Response of Specimen IJ-FC

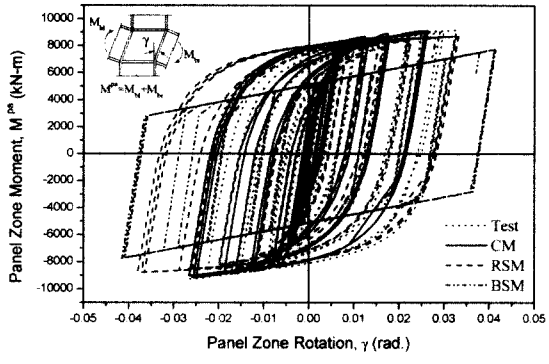

a) Panel Zone Response

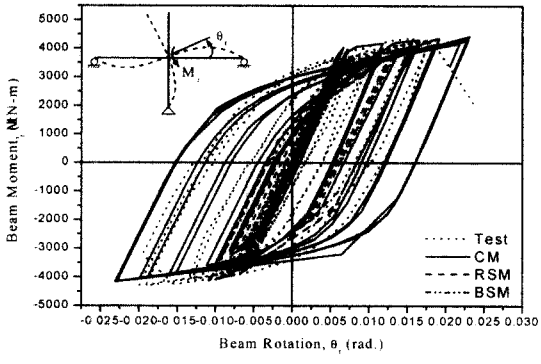

d) Beam Response

Fig. 8 Comparison of Model Predictions and Test Data for Local Response of Specimen UTA-FF

yielding to be confined to the composite beams, and the panel zones of the specimen were diagonally braced to remain elastic throughout the test, it is assumed that the columns and panel zones remain elastic during the analysis. As far as the monotonic behavior is concerned, the composite model overestimates the strength by about 6 %. The unloading elastic stiffnesses after the first half cycle of loading predicted by the composite model do not match well with that predicted by the test. However, for the rest of loading cycles the unloading elastic stiffnesses predicted by the analysis match well with that predicted by the test. The composite model exhibits more reasonable performance as a whole as compared to the bare steel models. The bare steel models underestimate the overall stiffness and strength of the test frame by about 40 % and 30 %, respectively.

The comparisons of local responses obtained by displacement control for the overall displacement of the subassemblages are presented in Figs. 7 and 8. The local panel zone responses for specimen IJ-FC are presented in Fig. 7. In Figs. 8a and 8b the local panel zone responses and beam responses for specimen UTA-FF are shown. From Fig. 7, it can be seen that all three models provide approximately the same panel zone rotations, which are little smaller than the experimental data. All three models showed that yielding was confined to the panel zone, as in the test. For specimen UTA-FF, the composite model predicted little smaller panel zone rotations than the experimental data, while the refined steel model predicted little larger panel zone rotations and the basic steel model provided much larger panel zone rotations. As far as the beam rotations are concerned, the composite model predicted little larger rotations than the experimental data, while the refined steel

model predicted much lesser rotations and the basic steel model showed very limited plastic rotations. All three models showed that there was no yielding in the columns. In Table 3 the plastic rotations predicted by the analytical models and the test are shown. From this table, it can be seen that all three models predicted approximately the same total plastic rotation (panel zone + beam + column) at the joint, which is little larger than the experimental data, as for specimen IJ-FC. However, the distribution of total plastic rotation at the joint between the beam and panel zone is significantly different for the three models. Consequently, for the same overall displacement, the three models predicted significantly different local plastic rotation demands. For the yielding to be properly distributed between the elements during the analysis, the analytical elements for the structural components should be able to accurately model the mechanical behavior of the structural components because even the displacement increment for infinitesimally small force increment may be large in the inelastic range due to a small stiffness. Since the composite model has the capability to more accurately define the mechanical behavior of the structural components, the local deformations predicted by it are much better than those obtained by the other models.

9. DYNAMIC ANALYSIS

In order to examine the effects of composite beam elements on predicted structural response, dynamic analyses were conducted for a six story, single bay steel moment frame subject to three strong ground motion records: the Sylmar record of the 1994 Northridge Earthquake, the Lucerne record of the 1992 Landers Earthquake, and SCT-1 record of the 1985 Mexico City Earthquake. In this study, the previous three models were applied: the composite,

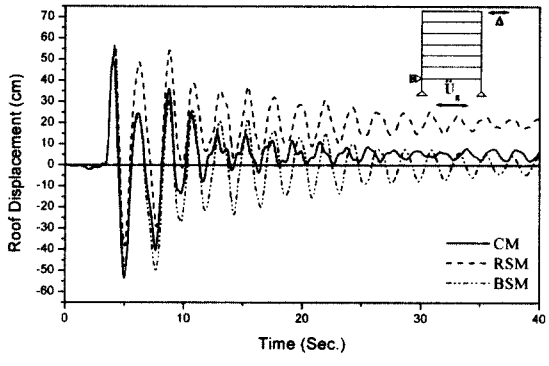

a) Roof Displacement

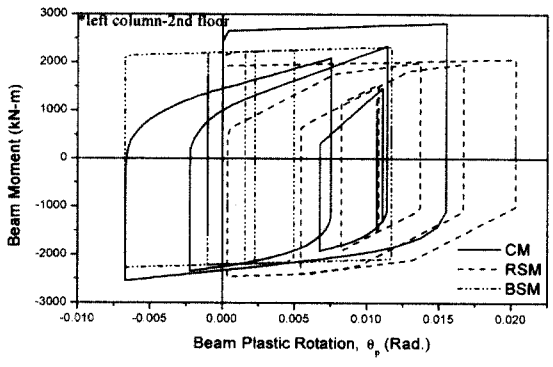

b) Beam Response

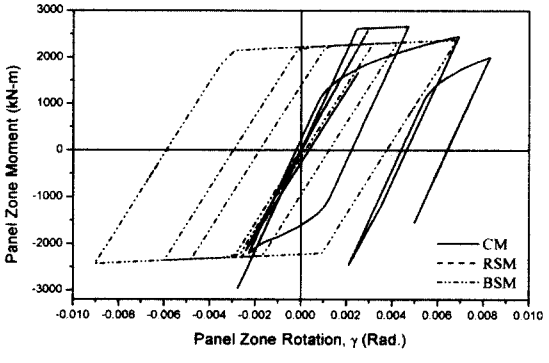

c) Panel Zone Response

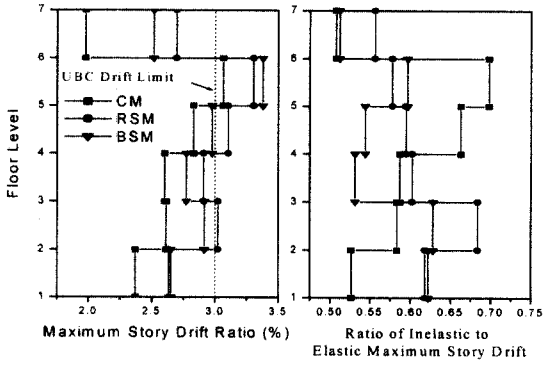

d) Maximum Story Drift Ratio

Fig. 9 Responses of Composite and Bare Steel Models for Sylmar Record

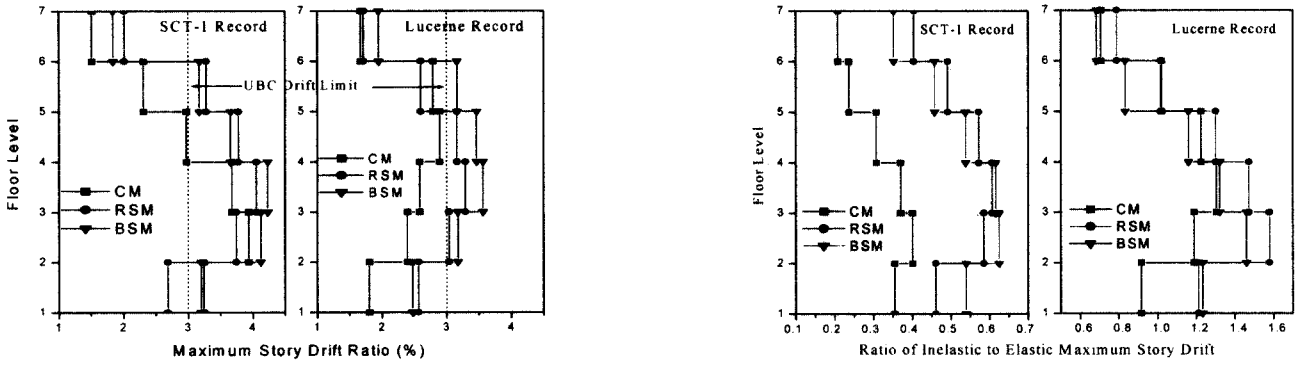

a) Maximum Story Drift Ratio

b) Ratio of Inelastic to Elastic Story Drift

Fig. 10 Responses of Composite and Bare Steel Models for SCT-1 and Lucerne Records

the refined steel, and the basic steel models. For all three models, mass and stiffness proportional damping coefficients were chosen to provide 2% of critical damping in the first and fourth modes and 40% doubler plate participation was used in the panel zone. The key features of the moment frame used in this study can be found in detail in the literature (Engelhardt and Kim 1995).

The response of models for the Sylmar record is shown in Fig. 9. This figure indicates that there are significant differences in the predicted response for the models. The differences are particularly large in the roof displacement histories (Fig. 9a) and in the beam plastic rotation plot (Fig. 9b) and in the panel zone response plot (Fig. 9c). In Figs. 9d and 10a the maximum story drift ratios for the three records are presented. The composite model provides stiffer behavior than the bare steel models for all three records and for the Lucerne record it shows significantly stiffer behavior. Figures 9d and 10b show the ratio of inelastic maximum story drift to elastic maximum story drift for the three records. This ratio of all three models is less than the value of 0.7 for the Sylmar and SCT-1 records, while for the Lucerne record the ratio is generally greater than the value of 1. For the Sylmar and SCT-1 records, there appear to be no consistent trends in the correlations of the ratios for the composite and bare steel models. For the SCT-1 record, this ratio for the composite model is about half of that for the bare steel models. This large difference can be attributed to the fact that this record has a large peak in its acceleration response spectrum at about a 2 second period, which is much closer to the first mode natural period of 1.909 seconds for the composite model than that of 2.214 seconds for the bare steel models. For the example frame, the difference of about 16% in the computed natural period is obtained due to the presence of composite slab. For all three records, there are large differences in the beam plastic rotations predicted by the three models at many joints on the order of 20% to 85% of each other without consistent trends.

The differences found in structural response predictions for the three models vary among the three records. There appear to be few, if any, consistent trends in how the composite model compares with the bare steel models among the three records. This suggests that the significance of effects of concrete slab on earthquake responses of MRFs is earthquake dependent. The differences in the predicted responses of the three models for the same ground motion is due both to differences in modeling inelastic behavior, as well as to differences in structural demands arising from the different natural periods of the models. When modeling steel moment frames, the accuracy of modeling for beams with composite slabs can have a significant effect on the locally and globally predicted responses.

10. CONCLUSION

The objective of the study in this paper was to develop a composite beam element to model steel beam with composite slabs during severe earthquake ground motions and to investigate the effects of composite slabs on seismic behavior of steel moment frames. The element can be considered as a one-component series hinge type model and it can reasonably model the strength, stiffness, pinching, and stiffness degradation of a composite beam. The composite beam element provides significantly better correlation with the test data as compared with the bare steel beam elements. The composite model can more accurately predict local deformation demands and overall response of structural systems under earthquake loading than the bare steel models. Composite slabs can significantly affect the global and local responses of steel moment frames. The significance of effects of concrete slab on earthquake responses of steel moment frames seems to be earthquake dependent.

APPENDIX. REFERENCES

1. duPlessis, D.P. and Daniels, J.H. (1972). "Experiments on composite beams under positive end moment." Rep. No. 374.2, Fritz Engrg. Lab., Lehigh University.
2. Engelhardt, M.D.,Kim, K.D., et al(1995). "Parametric studies on inelastic modeling of steel moment frames." Tech. Rep. SAC 95-05, SAC Joint Venture, Sacramento, CA.
3. Engelhardt, M.D., Fry, G.T., Jones, S., Venti, M. and Holliday, S. (2000). Behavior and design of radius-cut reduced beam section connections. Rep. No. SAC/BD-00/17, SAC Joint Venture, Sacramento, California.
4. Engelhardt, M.D. and Venti, M.J. (2000). Test of a free flange connection with a composite floor slab. Rep. No. SAC/BD-00/18, SAC Joint Venture, Sacramento, California.
5. Grant, J.A., Fisher, J.W., and Slutter, R.G. (1977). "Composite beams with formed steel deck." Engrg. Journal, AISC, 14(1), 24-43.
6. International Conference of Building Officials (1997). Uniform building code, ICBO, Whittier, CA.
7. Kanaan, A.E. and Powell, G.H. (1973). "DRAIN-2D: a general purpose computer program for dynamic analysis of inelastic plane structures-with user's guide." EERC Rep. No. 73/6 and 73/22, University of California, Berkeley.
8. Kim, K.D. and Engelhardt, M.D. (1995). "Development of analytical models for earthquake analysis of steel moment frames." Res. Rep. PMFSEL 95-2, Dept. of Civ. Engrg., The University of Texas at Austin, Texas.
9. Kim, K.D. and Engelhardt, M.D. (2000). "Beam-column element for nonlinear seismic analysis of steel frames." J. Struct. Engrg., ASCE, 126, 916-925.
10. Kim, K.D. and Engelhardt, M.D. (2002). "Monotonic and cyclic loading models for panel zones in steel moment frames." J. Const. Steel Research, 58(5-8), 605-635
11. Lee, S.J. (1987). "Seismic behavior of steel building structures with composite slabs." PhD thesis, Dept. of Civ. Engrg., Lehigh University, Bethlehem.
12. Ollgaard, J.G., Slutter, R.G., and Fisher, J.W. (1971). "Shear strength of stud connectors in lightweight and normal concrete." Engrg. Journal, AISC, 8(2), 55-64.
13. Przemieniecki, J.S. (1968). Theory of matrix structural analysis, McGraw-Hill Book Co., New York, N.Y.
14. Ricles, J.M. and Popov, E.P. (1987). "Dynamic analysis of seismically resistant eccentrically braced frames." EERC Rep. No. 87/07, University of California, Berkeley.
15. Slutter, R.G. and Driscoll, G.C. (1965). "Flexural strength of steel-concrete composite beams." J. Struct. Div., ASCE, 91(ST2).
16. Structural Engineers Association of California (1996). Recommended lateral force requirements, Sacramento, California.
17. Tagawa, Y., Aoki, H., and Kato, B. (1986). "Composite effect of concrete slabs and strength of composite girders under seismic loading." Proc., Pacific Struct. Steel Conf., New Zealand.
18. Tagawa, Y., Kato, B., and Aoki, H. (1989). "Behavior of composite beams in steel frame under hysteretic loading." J. Struct. Div., ASCE,

115(8), 2029-2045.

19. Uang, C.M. (1985). "Experimental and analytical study of the hysteretic behavior of steel composite girders." Rep. CE 299, Dept. of Civ. Engrg., University of California, Berkeley.

20. Wenk, T. and Daniels, J.H. (1977). "Composite assemblage experiments." Rep. No. 403.2, Fritz Engrg. Lab., Lehigh University, Bethlehem.

(접수일자 : 2002년 7월 11일)